# H trapping at the metastable cation vacancy in $\alpha$ -Ga<sub>2</sub>O<sub>3</sub> and $\alpha$ -Al<sub>2</sub>O<sub>3</sub>

Cite as: Appl. Phys. Lett. **120**, 192101 (2022); https://doi.org/10.1063/5.0094707 Submitted: 05 April 2022 • Accepted: 01 May 2022 • Published Online: 11 May 2022

Andrew Venzie, Amanda Portoff, DMichael Stavola, et al.







#### ARTICLES YOU MAY BE INTERESTED IN

Effects of temperature and oxygen partial pressure on electrical conductivity of Fe-doped  $\beta$ -Ga<sub>2</sub>O<sub>3</sub> single crystals

Applied Physics Letters 120, 182101 (2022); https://doi.org/10.1063/5.0093588

Two inch diameter, highly conducting bulk  $\beta$ -Ga<sub>2</sub>O<sub>3</sub> single crystals grown by the Czochralski method

Applied Physics Letters 120, 152101 (2022); https://doi.org/10.1063/5.0086996

A review of Ga<sub>2</sub>O<sub>3</sub> materials, processing, and devices

Applied Physics Reviews 5, 011301 (2018); https://doi.org/10.1063/1.5006941

Lock-in Amplifiers up to 600 MHz



ZurichInstruments







# H trapping at the metastable cation vacancy in $\alpha$ -Ga<sub>2</sub>O<sub>3</sub> and $\alpha$ -Al<sub>2</sub>O<sub>3</sub>

Cite as: Appl. Phys. Lett. **120**, 192101 (2022); doi: 10.1063/5.0094707 Submitted: 5 April 2022 · Accepted: 1 May 2022 ·

Published Online: 11 May 2022







Andrew Venzie,¹ Amanda Portoff,¹ Michael Stavola,¹.a¹ (p) W. Beall Fowler,¹ (p) Jihyun Kim,² (p) Dae-Woo Jeon,³ (p) Ji-Hyeon Park,³ and Stephen J. Pearton⁴ (p)

#### **AFFILIATIONS**

- <sup>1</sup>Department of Physics, Lehigh University, Bethlehem, Pennsylvania 18015, USA
- <sup>2</sup>School of Chemical and Biological Engineering, Seoul National University, Seoul 08826, South Korea
- <sup>3</sup>Korea Institute of Ceramic Engineering & Technology, Jinju 52851, South Korea
- Department of Materials Science and Engineering, University of Florida, Gainesville, Florida 32611, USA

#### **ABSTRACT**

 $\alpha$ -Ga<sub>2</sub>O<sub>3</sub> has the corundum structure analogous to that of  $\alpha$ -Al<sub>2</sub>O<sub>3</sub>. The bandgap energy of  $\alpha$ -Ga<sub>2</sub>O<sub>3</sub> is 5.3 eV and is greater than that of  $\beta$ -Ga<sub>2</sub>O<sub>3</sub>, making the  $\alpha$ -phase attractive for devices that benefit from its wider bandgap. The O–H and O–D centers produced by the implantation of H<sup>+</sup> and D<sup>+</sup> into  $\alpha$ -Ga<sub>2</sub>O<sub>3</sub> have been studied by infrared spectroscopy and complementary theory. An O–H line at 3269 cm<sup>-1</sup> is assigned to H complexed with a Ga vacancy (V<sub>Ga</sub>), similar to the case of H trapped by an Al vacancy (V<sub>Al</sub>) in  $\alpha$ -Al<sub>2</sub>O<sub>3</sub>. The isolated V<sub>Ga</sub> and V<sub>Al</sub> defects in  $\alpha$ -Ga<sub>2</sub>O<sub>3</sub> and  $\alpha$ -Al<sub>2</sub>O<sub>3</sub> are found by theory to have a "shifted" vacancy-interstitial-vacancy equilibrium configuration, similar to V<sub>Ga</sub> in  $\beta$ -Ga<sub>2</sub>O<sub>3</sub>, which also has shifted structures. However, the addition of H causes the complex with H trapped at an unshifted vacancy to have the lowest energy in both  $\alpha$ -Ga<sub>2</sub>O<sub>3</sub> and  $\alpha$ -Al<sub>2</sub>O<sub>3</sub>.

Published under an exclusive license by AIP Publishing. https://doi.org/10.1063/5.0094707

 $\beta\text{-}Ga_2O_3$  is an ultrawide ( $\cong 4.8\,\text{eV}$ ) bandgap semiconductor that has been attracting much attention for high-power, deep-UV, and extreme environment applications. While the  $\beta\text{-}$ phase is the most thermally stable  $^{5-9}$  of  $Ga_2O_3$ , other metastable phases can be grown that are sufficiently stable to be used to fabricate devices. Of particular interest here is the  $\alpha\text{-}Ga_2O_3$  phase that has a bandgap energy of 5.3 eV,  $^{3.7}$  exceeding that of the  $\beta\text{-}$ phase.

 $\alpha\text{-}Ga_2O_3$  has the corundum crystal structure  $^{5,6,11}$  analogous to  $\alpha\text{-}Al_2O_3,^{12}$  which makes sapphire a suitable substrate for the epitaxial growth of  $\alpha\text{-}Ga_2O_3$ . Despite a lattice mismatch between  $\alpha\text{-}Ga_2O_3$  and  $\alpha\text{-}Al_2O_3$  of 4.6% (a-axis) and 3.9% (c-axis),  $\alpha\text{-}Ga_2O_3$  has been grown on (0001) sapphire substrates by several epitaxial growth methods. Of these, halide vapor phase epitaxy (HVPE) is advantageous for the growth of thick device layers because of its rapid growth rate.  $^{1,3,7,9}$ 

The hydrogen impurity impacts the conductivity of semiconducting oxides, where it can act as a shallow donor or can passivate defects and impurities.  $^{13-15}$  In the present work, OH and OD centers are investigated in the  $\alpha$ -phase of  $Ga_2O_3$  by infrared (IR) spectroscopy and complementary theory.

Because  $\alpha$ -Ga<sub>2</sub>O<sub>3</sub> and  $\alpha$ -Al<sub>2</sub>O<sub>3</sub> have analogous crystal structures, the IR spectrum and structure of the isolated OH center in sapphire

are also considered in this Letter. In the corundum structure  $^{12}$  of  $\alpha$ -Al<sub>2</sub>O<sub>3</sub>, each Al atom is bonded to six oxygen atoms, where there are three equivalent O atoms having long Al–O bonds and three equivalent O atoms that have short Al–O bonds.

A recent paper by Balan contains references for OH centers in both natural and synthetic  $\alpha\text{-}\mathrm{Al}_2\mathrm{O}_3$  and a discussion of models for these centers.  $^{16}$  Of particular interest to us are OH and OD centers complexed with native defects that do not involve additional impurities.

Experiments by Engstrom *et al.*, <sup>17</sup> Moon and Phillips, <sup>18</sup> and Ramiriez *et al.* <sup>19</sup> have examined the polarization properties of the OH vibrational lines in  $\alpha$ -Al<sub>2</sub>O<sub>3</sub> to provide structure sensitive information about the defects. OH centers of interest to us have vibrational frequencies near 3200 cm<sup>-1</sup> and transition moment directions in or near the basal plane of the corundum structure. The corresponding OD modes have frequencies near 2400 cm<sup>-1</sup>. <sup>17</sup>

Recent theory performed by Thienprasert *et al.* identified a stable defect structure in  $\alpha$ -Al<sub>2</sub>O<sub>3</sub> consisting of an OH complexed with an Al vacancy (V<sub>Al</sub>) with a vibrational frequency and a transition moment direction consistent with experiment.<sup>20</sup> Additional defects containing two or three H atoms complexed with V<sub>Al</sub> were also studied.<sup>20</sup> In spite

a) Author to whom correspondence should be addressed: michael.stavola@Lehigh.edu

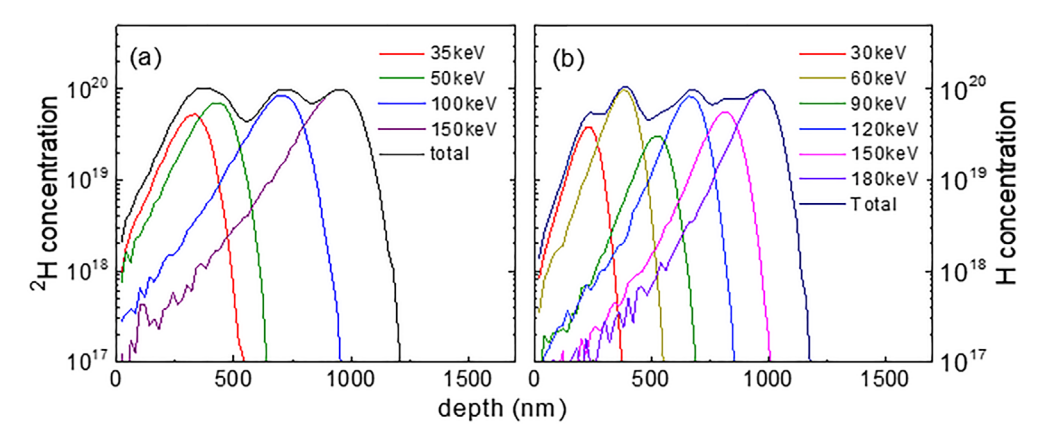


**FIG. 1.** Ion depth profiles calculated with SRIM for  $\alpha$ -Ga<sub>2</sub>O<sub>3</sub> samples implanted with (a) D<sup>+</sup> and (b) H<sup>+</sup> with multiple energies and doses to give ion concentrations of approximately  $10^{20}$  cm<sup>-3</sup> with a depth compatible with the 1200 nm epilayer thickness.

of long-standing interest, defect structures for specific OH vibrational lines in  ${\rm Al_2O_3}$  remain controversial with there being uncertainty about whether additional transition metal impurities are present. <sup>16</sup>

The  $\alpha$ -Ga $_2$ O $_3$  samples for our experiments were 1200 nm-thick, undoped epitaxial layers grown on (0001) sapphire substrates by the halide-vapor-phase-epitaxy (HVPE) method at the Korean Institute of Ceramic Engineering and Technology. Samples were implanted with multiple energies and doses of H $^+$  and/or D $^+$  to produce hydrogenated and deuterated layers approximately 1200 nm thick with H and D concentrations of  $10^{20}$  cm $^{-3}$ . The Stopping and Range of Ions in Matter (SRIM) profiles of the H and D concentrations vs depth are shown in Fig. 1.

IR absorption spectra $^{21,22}$  were measured with a Nicolet iS50 Fourier transform IR spectrometer equipped with a CaF<sub>2</sub> beam splitter and a liquid N<sub>2</sub>-cooled InSb detector. Samples were cooled for our measurements with liquid N<sub>2</sub> in a Helitran continuous flow cryostat. (Cooling to 5 K did not cause the observed IR lines in implanted

samples to narrow further.) Annealing treatments were performed in a tube furnace in a flowing Ar ambient.

Figure 2 shows IR spectra for a 1200 nm thick epilayer of  $\alpha$ -Ga<sub>2</sub>O<sub>3</sub> implanted with H<sup>+</sup> and D<sup>+</sup> with multiple energies and doses to give the SRIM profiles that are shown in Fig. 1. Figure 2(a) also shows a sample prepared by implanting D<sup>+</sup> into its reverse side, i.e., into its sapphire substrate. The implantation of D<sup>+</sup> into the Al<sub>2</sub>O<sub>3</sub> substrate produced an IR line at 2440 cm<sup>-1</sup> (77 K) that has been attributed previously to an OD stretching mode [Fig. 2(a)] with its transition moment in the basal plane of the corundum crystal structure of Al<sub>2</sub>O<sub>3</sub>. <sup>17,19</sup>

Theory has suggested that OD modes in  $\alpha$ -Al<sub>2</sub>O<sub>3</sub> near 2400 cm<sup>-1</sup> are due to complexes of OD with V<sub>Al</sub>.<sup>20</sup> However, as noted above, several such modes have been observed in bulk  $\alpha$ -Al<sub>2</sub>O<sub>3</sub>, and it has also been suggested that additional impurities may also be involved in these defects. <sup>16</sup> Our results for H<sup>+</sup> and D<sup>+</sup> implanted into  $\alpha$ -Al<sub>2</sub>O<sub>3</sub> with concentrations of approximately  $10^{20}$  cm<sup>-3</sup> are consistent with the

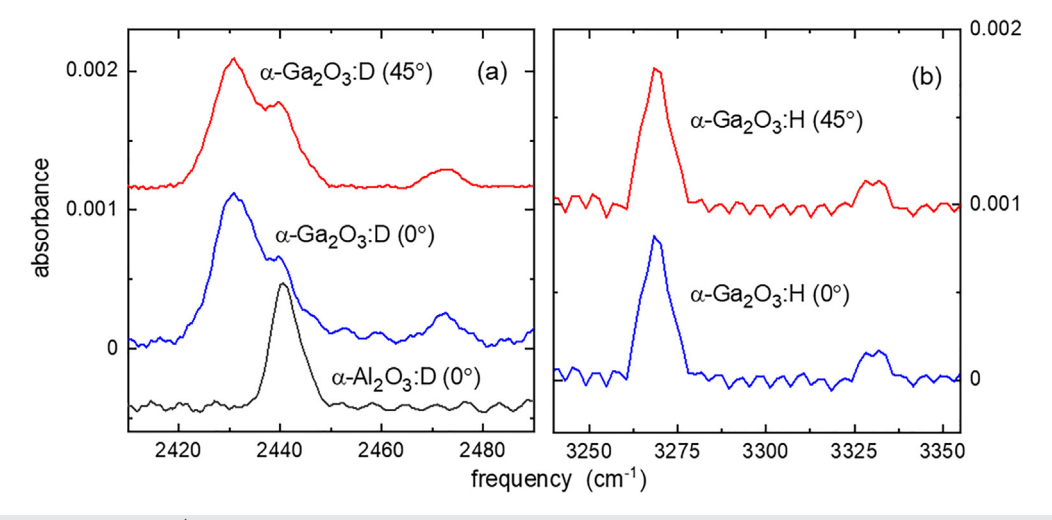


**FIG. 2.** IR spectra (77 K, resolution 1 cm<sup>-1</sup>) for  $\alpha$ -Ga<sub>2</sub>O<sub>3</sub> epitaxial layers implanted with (a) D<sup>+</sup> and (b) H<sup>+</sup>. Spectra labeled 0° were for IR spectra measured with the light at normal incidence. Spectra labeled 45° were for IR spectra measured with the sample rotated 45° from the normal direction. The spectrum in panel (a) labeled  $\alpha$ -Al<sub>2</sub>O<sub>3</sub>:D was measured for a sample that had D<sup>+</sup> implanted into the sapphire substrate rather than the epilayer. (Spectra have been displaced vertically for clarity.)

line at  $2440\,\mathrm{cm}^{-1}$  being due to an isolated OD-V<sub>Al</sub> center because the implant profile used here should greatly exceed the concentrations of unintentional transition-metal impurities in undoped transparent sapphire substrates. (The IR line intensities are also consistent with the nominal D<sup>+</sup> implantation dose and a reasonable value for the effective charge for the oscillating defect.  $^{21}$ )

The spectrum for  $D^+$  implanted into the  $\alpha$ -Ga<sub>2</sub>O<sub>3</sub> epilayer shows 3 IR lines. There are two new lines at 2431 and 2472 cm<sup>-1</sup>. The line at 2440 cm<sup>-1</sup> that is also observed is consistent with OD in Al<sub>2</sub>O<sub>3</sub>, showing that the  $D^+$  implant extends into the substrate of the sample, consistent with the SRIM profile for D (i.e., <sup>2</sup>H) shown in Fig. 1(a).

The spectrum for  $H^+$  implanted into  $\alpha$ -Ga<sub>2</sub>O<sub>3</sub> shows two IR lines at 3269 and 3331 cm<sup>-1</sup> that correspond to the two new OD lines seen in Fig. 2(a). In this case, the implanted  $H^+$  does not reach the sapphire substrate and a line due to OH in Al<sub>2</sub>O<sub>3</sub> does not appear. The ratios of the frequencies of the corresponding lines shown in Figs. 2(a) and 2(b) are  $\omega_H/\omega_D\cong 1.345$ , consistent with their assignments to the vibrational modes of H and D bonded to an atom with light mass like O.<sup>21</sup> The new OH (OD) lines that we have discovered for  $H^+$  (D<sup>+</sup>) implanted  $\alpha$ -Ga<sub>2</sub>O<sub>3</sub> lie approximately 180 (120) cm<sup>-1</sup> lower in frequency than the OH (OD) lines observed recently for H and D in  $\beta$ -Ga<sub>2</sub>O<sub>3</sub>.<sup>23,24</sup>

The spectra shown in Fig. 2 labeled  $(0^{\circ})$  were measured with the incident light at normal incidence to the (0001) plane of the sample. Spectra were also measured for samples rotated  $45^{\circ}$  from normal incidence to investigate whether any IR lines were produced with transition moments with a dominant component along the c-axis. No such lines were observed in our experiments.

Samples were also prepared by the co-implantation of both  $H^+$  and  $D^+$  into an  $\alpha$ -Ga<sub>2</sub>O<sub>3</sub> layer. In this case, the OH and OD lines seen in Figs. 2(a) and 2(b) were all produced in this sample. No additional lines that might arise from defects that contain both H and D were resolved, perhaps due to the large line widths of the lines.

The  $\alpha\text{-}Ga_2O_3$  sample implanted with  $D^+$  whose multi-line spectrum is shown in Fig. 2(a) was subjected to a series of sequential 30 min anneals at temperatures beginning at  $100\,^{\circ}\text{C}$  and increasing in  $50\,^{\circ}\text{C}$  increments (Fig. 3). The IR line at  $2472\,\text{cm}^{-1}$  was annealed away at  $200\,^{\circ}\text{C}$ . The line at  $2431\,\text{cm}^{-1}$  was eliminated at an annealing temperature of  $350\,^{\circ}\text{C}$ .

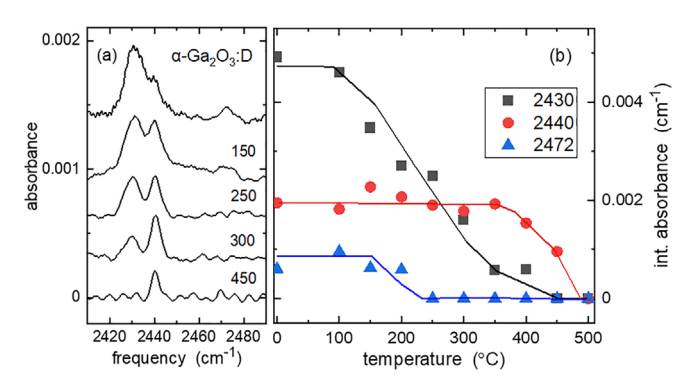


**FIG. 3.** Panel (a) shows IR absorption spectra (77 K, resolution 1 cm $^{-1}$ ) for an  $\alpha$ -Ga<sub>2</sub>O<sub>3</sub> epitaxial layer implanted with D $^+$  at room temperature. The top spectrum is for the as-implanted sample. Panel (b) shows the integrated absorbances for the IR lines with the given frequencies vs annealing temperature. Lines are drawn to guide the eye.

The line at  $2440\,\mathrm{cm}^{-1}$  due to the OD-V<sub>AI</sub> complex in the sapphire substrate was eliminated at  $450\,^{\circ}$ C. These results show that the  $2431,\,2440,\,$  and  $2472\,\mathrm{cm}^{-1}$  lines arise from different OD centers. The temperatures for which the defects are eliminated also show that the corresponding OH centers with similar chemical properties, if unintentionally present in device materials, can be eliminated by annealing at temperatures where the  $\alpha$ -Ga<sub>2</sub>O<sub>3</sub> host remains thermally stable.

In order to investigate the expected properties of OH defects in the alpha phases of  $Al_2O_3$  and  $Ga_2O_3$ , we have carried out theoretical calculations on 120 atom supercells using the CRYSTAL17 code<sup>25</sup> with B3LYP hybrid exchange<sup>26</sup> and default relaxation criteria. Gaussian basis functions were of the type 311p(1) for H (Ref. 27), 8411 for O (Ref. 28), 864111d41 for Ga (Ref. 29), and 8511G\* for Al (Ref. 30). This approach has proven successful for defect studies in a number of oxides,  $^{31-33}_{31-31}$  most recently  $\beta$ -Ga<sub>2</sub>O<sub>3</sub>.  $^{23,24,34}_{31-31}$ 

For both of the present alpha-phase systems, we calculate equilibrium coordinates for the perfect crystal and use these throughout in defining unit cell parameters for defect calculations. These calculated coordinates agree with the experimental values to within  $\approx 1\%$ .  $^{1.3,11,12}$  Perhaps fortuitously, computed bandgaps agree with experiment to within  $0.2\,\mathrm{eV}$ .  $^{3,7,35}$ 

Figure 4 shows a portion of the corundum structure viewed perpendicular to the c axis. This structure has threefold rotational symmetry about the c axis, and the oxygens (to which H will attach) form equilateral triangles centered on the c axis. The two types of triangles are denoted in Fig. 4 by red (larger) and yellow (smaller), whose oxygen separations differ by  $\approx 0.4$  Å. Figure 4(a) represents the perfect structure, Fig. 4(b) illustrates a plain, unrelaxed cation vacancy, and Fig. 4(c) represents a vacancy-interstitial-vacancy complex that has been generally labeled as a transition state configuration.

We include the structure of Fig. 4(c) because the accumulation of theoretical and experimental work  $^{23,24,34,38-43}$  on the Ga(1) vacancy in  $\beta$ -Ga<sub>2</sub>O<sub>3</sub> provides convincing evidence that such shifted configurations represent the dominant framework for understanding both the "pure" Ga(1) vacancy and the vacancy that has trapped one or more H. In the  $\beta$ -Ga<sub>2</sub>O<sub>3</sub> structure, there are in fact two distinct vacancy-interstitial-vacancy configurations,  $^{38,39}$  one preferred for the pure defect in the -3 charge state, the other preferred after trapping a hole  $^{42,43}$  or one or more H.  $^{23,24}$ 

Indeed, our present calculations on both  $\alpha\text{-}Al_2O_3$  and  $\alpha\text{-}Ga_2O_3$  predict, for the -3 charge state, that the configuration of Fig. 4(c), namely, the shifted vacancy-interstitial-vacancy complex, is lower in energy than the simple vacancy [Fig. 4(b)], by 0.7 eV for  $Al_2O_3$  and by 0.6 eV for  $Ga_2O_3$ . These magnitudes are similar to results obtained by us  $^{23,24}$  and by others  $^{38,39}$  for the shifted structures in  $\beta\text{-}Ga_2O_3$ .

Studies of cation-vacancy diffusion in corundum oxides  $^{44-46}$  have noted the importance of the vacancy-interstitial-vacancy configuration as part of the process, some noting its closeness in energy to the unrelaxed vacancy, and in fact (although the implications of this point are not followed through), the non-hybrid density functional theory (DFT) calculation of Lei and Wang  $^{45}$  indicates that what they call the transition state is lower than the unshifted state for all charges, by as much as  $0.8\,\mathrm{eV}$  for the -3 charge state, a result consistent with our computed value of  $0.7\,\mathrm{eV}$ .

Indeed, we suggest, based on the knowledge obtained for  $\beta$ -Ga<sub>2</sub>O<sub>3</sub>, that the "cation vacancy" in both Al<sub>2</sub>O<sub>3</sub> and Ga<sub>2</sub>O<sub>3</sub>, and perhaps in other corundum-structured oxides, is in fact *the* vacancy-interstitial-vacancy complex in the -3 charge state—that is, the

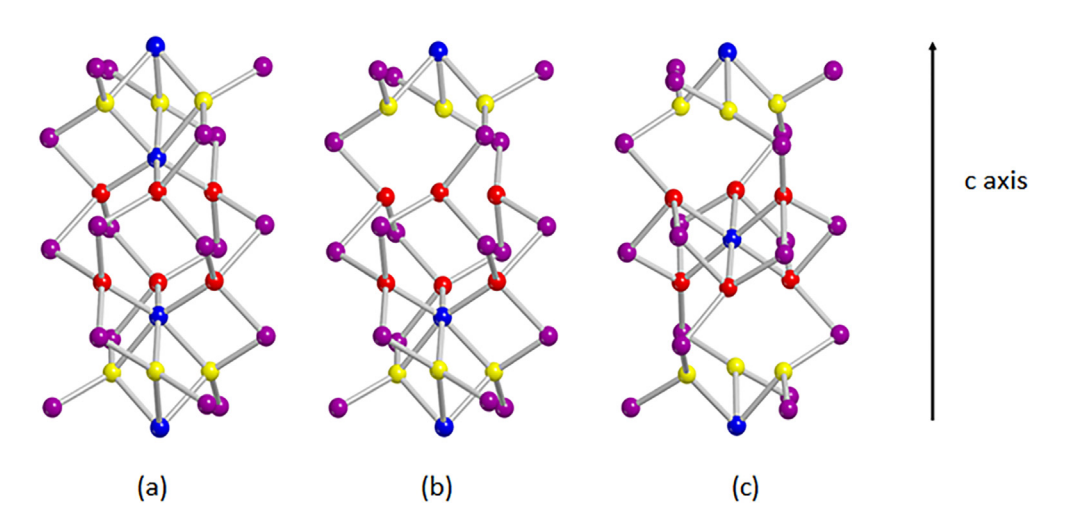


FIG. 4. Portions of the 120-atom supercell used in the present work. Cations (Al or Ga) are shown in purple or blue; the blue cations indicate the c axis direction at the center of the threefold structure. Red and yellow represent oxygens; in each equilateral triangle, the red oxygens are about 0.4 Å farther apart than the yellow oxygens. (a) represents the perfect structure, (b) an unrelaxed cation vacancy, and (c) a cation vacancy with a neighboring cation shifted to an interstitial site with two neighboring vacancies. These figures were constructed using MOLDRAW<sup>36</sup> and POV-Ray.<sup>37</sup>

"transition state" is actually the equilibrium configuration of the cation vacancy. This means that a number of vacancy properties that had been assigned to the plain vacancy configuration will need to be revisited.

But what of the trapped H defect? Here, we find that when the vacancy includes a trapped H, the plain, or unshifted, vacancy configuration is favored, by 0.5 eV for  $\text{Al}_2\text{O}_3$  and by 0.34 eV for  $\text{Ga}_2\text{O}_3$ . Thus, in treating H-related defects, we consider only the plain vacancy [Fig. 4(b)].

A large amount of experimental and theoretical work has been carried out by others  $^{16-20,47-51}$  on H in  $\alpha\text{-Al}_2O_3$ , and to the extent that they overlap, our calculations generally support the consensus of these results. We agree that a trapped interstitial H is not a tenable model for the primary  $\approx\!3282$  (2440) cm $^{-1}$  OH (OD) line, as that model predicts an angle between the c axis and the O–H transition moment of  $60^\circ$  or less and an elongated O–H bond associated with a low vibrational frequency. We also agree that a H trapped at an unshifted Al vacancy will prefer to attach to an O on the larger triangle (red) rather than an O on the smaller triangle (yellow). Furthermore, on the larger triangle, we find the O–H transition moment to make an angle of  $82^\circ$  with the c axis, while on the smaller triangle, the corresponding angle is  $38^\circ$ . These structures are shown in Fig. 5.

Because there are six candidate O sites on which H or D may be trapped, there may be many combinations of 2 or 3 H or D defects, as noted in Ref. 20. These will lead to additional vibrational lines, some of which will be oriented nearly perpendicular to the c axis and others making a small angle with respect to c. For example, if both sites in Fig. 5 are occupied, one O–H axis will be 85° with respect to c, the other 35°—essentially the superposition of Figs. 5(a) and 5(b). In general, the calculated anharmonic vibrational frequency associated with D trapped on the smaller triangle (yellow) will be of order 200 cm<sup>-1</sup> less than that for D on the (more favored) larger triangle (red).

Regarding  $\alpha$ -Ga<sub>2</sub>O<sub>3</sub>, our results are found to be very similar to those described above for  $\alpha$ -Al<sub>2</sub>O<sub>3</sub>, suggesting that the corundum structure largely governs the physics that we are exploring. Most

pertinent to the experimental results for the 2431 and 3269 cm<sup>-1</sup> lines discussed above, a single H or D is predicted to be trapped at a Ga vacancy by an O on a larger triangle (red) with an O–H axis 83° from the c axis, with trapping by an O on a smaller (yellow) triangle less favored energetically and with an O–H angle 38° with respect to c. The computed vibrational frequency (2460 cm<sup>-1</sup>) for D trapped on a larger triangle, which should correspond to the observed result, is lower than values obtained for  $\beta\text{-Ga}_2\text{O}_3^{23,24}$  by  $\sim\!100$  to 150 cm<sup>-1</sup>, a result consistent with experiment.

Similar to D in  $\alpha$ -Al<sub>2</sub>O<sub>3</sub>, <sup>20</sup> defects that contain two or three D are possible in Ga<sub>2</sub>O<sub>3</sub> and may explain the weak OD line observed at 2472 cm<sup>-1</sup>. A configuration with two D on a larger triangle and an

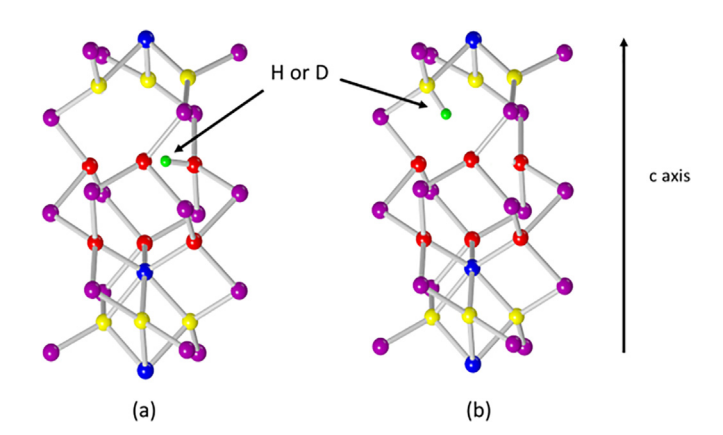


**FIG. 5.** Possible locations of H or D trapped at an unrelaxed Al or Ga vacancy [see Fig. 4(b)]. Color coding as in Fig. 4. (a) represents the energetically favored structure, with H trapped at an O in a larger triangle, and as shown with the O–H axis nearly perpendicular to the c axis. (b) represents the less favored structure with H trapped at an O in a smaller triangle; the O–H axis makes an angle  $\approx 38^\circ$  with respect to the c axis. These figures were constructed using MOLDRAW<sup>36</sup> and POV-Rav<sup>37</sup>

alternative configuration with one D on a larger triangle and a second on a smaller triangle have energies that differ by less than 0.1 eV and essentially degenerate. The former configuration is predicted to have two OD modes at higher frequencies than the single OD center (2507 and 2564 cm<sup>-1</sup>). The latter is predicted to have one OD mode at higher frequency and a second at lower frequency than the single OD center (2501 and 2233 cm<sup>-1</sup>). The OD line at 2472 cm<sup>-1</sup> seen by experiment is weak in the thin implanted layers studied here, and additional lines have not been observed, so both configurations suggested by theory remain as possibilities.

We finally note that for both materials, a H trapped at the vacancy-interstitial-vacancy complex will attach to an O on a smaller (yellow) triangle and will have an O–H angle of order 35° with respect to the c axis, clearly not observed (and not favored energetically).

In summary, an O–H (O–D) center with an IR line at 3269 (2431) cm $^{-1}$  produced by the implantation of  $H^+$  (D $^+$ ) into  $\alpha\text{-}Ga_2O_3$  has been discovered by IR spectroscopy. Theory assigns the O–H line at 3269 cm $^{-1}$  to H complexed with  $V_{Ga}$ , similar to the case of H complexed with  $V_{Al}$  in  $\alpha\text{-}Al_2O_3$ . Theory also finds that the isolated  $V_{Ga}$  and  $V_{Al}$  defects in  $\alpha\text{-}Ga_2O_3$  and  $\alpha\text{-}Al_2O_3$ , respectively, have a shifted vacancy-interstitial-vacancy configuration, similar to  $V_{Ga}$  in  $\beta\text{-}Ga_2O_3$ , which also has shifted structures. However, the addition of H causes a complex with H trapped at an unshifted vacancy, that is metastable in the absence of H, to have lowest energy in both  $\alpha\text{-}Ga_2O_3$  and  $\alpha\text{-}Al_2O_3$ . Defects that may contain more than one H or D atom have also been investigated.

The work at Lehigh University was supported by NSF Grant No. DMR 1901563 (James Edgar). The work in South Korea was supported by Basic Science Research Program through the National Research Foundation of Korea (NRF) funded by the Ministry of Education (Nos. 2018R1D1A1B07048429 and 2020M3H4A3081799). The work at UF was performed as part of Interaction of Ionizing Radiation with Matter University Research Alliance (IIRM-URA), sponsored by the Department of the Defense, Defense Threat Reduction Agency under Award No. HDTRA1-20-2-0002 (Jacob Calkins). The content of the information does not necessarily reflect the position or the policy of the federal government, and no official endorsement should be inferred. The work at UF was also supported by NSF No. DMR 1856662 (James Edgar). Portions of this research were conducted on Research Computing resources provided by Lehigh University supported by the NSF Award No. 2019035.

## **AUTHOR DECLARATIONS**

# **Conflict of Interest**

The authors have no conflicts to disclose.

### **DATA AVAILABILITY**

The data that support the findings of this study are available from the corresponding author upon reasonable request.

#### **REFERENCES**

- <sup>1</sup>S. I. Stepanov, V. I. Nikolaev, V. E. Bougrov, and A. E. Romanov, Rev. Adv. Mater. Sci. 44, 63 (2016).
- <sup>2</sup>M. Higashiwaki, A. Kuramata, H. Murakami, and Y. Kumagai, J. Phys. D **50**, 333002 (2017).

- <sup>3</sup>S. J. Pearton, J. Yang, P. H. Cary, F. Ren, J. Kim, M. J. Tadjer, and M. A. Mastro, Appl. Phys. Rev. 5, 011301 (2018).
- <sup>4</sup>J. Zhang, J. Shi, D.-C. Qi, L. Chen, and K. H. L. Zhang, APL Mater. 8, 020906 (2020).
- <sup>5</sup>R. Roy, V. G. Hill, and E. F. Osborn, J. Am. Chem. Soc. **74**, 719 (1952).
- <sup>6</sup>H. Y. Playford, A. C. Hannon, E. R. Barney, and R. I. Walton, Chem. Eur. J. 19, 2803 (2013).
- <sup>7</sup>E. Ahmadi and Y. Oshima, J. Appl. Phys. **126**, 160901 (2019).
- <sup>8</sup>I. Cora, F. Mezzadri, F. Boschi, M. Bosi, M. Čaplovičová, G. Calestani, I. Dódony, B. Pécz, and R. Fornari, Cryst. Eng. Commun. **19**, 1509 (2017).
- <sup>9</sup>S. Shapenkov, O. Vyvenko, V. Nikolaev, S. Stepanov, A. Pechnikov, M. Scheglov, and G. Varygin, Phys. Status Solidi B **259**, 2100331 (2022).
- <sup>10</sup>H. Son, Y. Choi, J.-H. Park, B. Ryu, and D.-W. Jeon, ECS J. Solid State Sci. Technol. 9, 055005 (2020).
- <sup>11</sup>M. Marezio and J. P. Remeika, J. Chem. Phys. **46**, 1862 (1967).
- <sup>12</sup>R. E. Newnham and Y. M. de Haan, Z. Kristallogr. 117, 235 (1962).
- <sup>13</sup>P. D. C. King and T. D. Veal, J. Phys.: Condens. Matter **23**, 334214 (2011).
- <sup>14</sup>M. D. McCluskey, M. C. Tarun, and S. T. Teklemichael, J. Mater. Res. 27, 2190 (2012).
- <sup>15</sup>M. Stavola, W. B. Fowler, Y. Qin, P. Weiser, and S. J. Pearton, Ga<sub>2</sub>O<sub>3</sub>, Technology, Devices and Applications, edited by S. J. Pearton, F. Ren, and M. Mastro (Elsevier, Amsterdam, 2018), Chap. 9, p. 191.
- <sup>16</sup>E. Balan, Eur. J. Miner. **32**, 457 (2020).
- <sup>17</sup>H. Engstrom, J. Bates, J. C. Wang, and M. M. Abraham, Phys. Rev. B 21, 1520 (1980).
- <sup>18</sup>A. R. Moon and M. R. Phillips, Appl. Spectrosc. **45**, 1051 (1991).
- <sup>19</sup>R. Ramirez, I. Colera, R. González, Y. Chen, and M. R. Kokta, Phys. Rev. B 69, 014302 (2004).
- <sup>20</sup>J. T. Thienprasert, A. Boonchun, P. Reunchan, and S. Limpijumnong, Phys. Rev. B 95, 134103 (2017).
- <sup>21</sup>M. Stavola, *Identification of Defects in Semiconductors*, edited by M. Stavola (Academic, Boston, 1998), Vol. 51B, Chap. 3, p. 153.
- <sup>22</sup>M. Stavola and W. B. Fowler, J. Appl. Phys. **123**, 161561 (2018).
- <sup>23</sup>P. Weiser, M. Stavola, W. B. Fowler, and Y. Qin, Appl. Phys. Lett. 112, 232104 (2018).
- <sup>24</sup>Y. Qin, M. Stavola, W. B. Fowler, P. Weiser, and S. J. Pearton, ECS J. Solid State Sci. Technol. 8, Q3103 (2019).
- <sup>25</sup>R. Dovesi, A. Erba, R. Orlando, C. M. Zicovich-Wilson, B. Civalleri, L. Maschio, M. Rérat, S. Casassa, J. Baima, S. Salustro, and B. Kirtman, "Quantum-mechanical condensed matter simulations with CRYSTAL," WIRES Comput. Mol. Sci. 8, e1360 (2018).
- <sup>26</sup>A. D. Becke, J. Chem. Phys. **98**, 5648 (1993).
- <sup>27</sup>R. Krishnan, J. S. Binkley, R. Seeger, and J. A. Pople, J. Chem. Phys. **72**, 650 (1980).
- <sup>28</sup>J. E. Jaffe and A. C. Hess, Phys. Rev. B **48**, 7903 (1993).
- <sup>29</sup>R. Pandey, J. E. Jaffe, and N. M. Harrison, J. Phys. Chem. Solids 55, 1357 (1994).
- 30 M. Catti, G. Valerio, R. Dovesi, and M. Causà, Phys. Rev. B 49, 14179 (1994).
- <sup>31</sup>F. Bekisli, M. Stavola, W. B. Fowler, L. Boatner, E. Spahr, and G. Lübke, Phys. Rev. B 84, 035213 (2011).
- <sup>32</sup>F. Bekisli, W. B. Fowler, and M. Stavola, Phys. Rev. B **86**, 155208 (2012).
- 33W. Yin, K. Smithe, P. Weiser, M. Stavola, W. B. Fowler, L. Boatner, S. J. Pearton, D. C. Hays, and S. G. Koch, Phys. Rev. B 91, 075208 (2015).
- 34W. B. Fowler, M. Stavola, Y. Qin, and P. Weiser, Appl. Phys. Lett. 117, 142101
- 35M. L. Bortz and R. H. French, Appl. Phys. Lett. 55, 1955 (1989).
- <sup>36</sup>See P. Ugliengo, http://moldraw.unito.it for "MOLDRAW" (2006).
- 37 See http://povray.org for "POV-Ray."
- <sup>58</sup>J. B. Varley, H. Peelaers, A. Janotti, and C. G. Van de Walle, J. Phys.: Condens. Matter 23, 334212 (2011).
- <sup>39</sup> A. Krytsos, M. Matsubara, and E. Bellotti, Phys. Rev. B **95**, 245202 (2017).
- <sup>40</sup>J. M. Johnson, Z. Chen, J. B. Varley, C. M. Jackson, E. Farzana, Z. Zhang, A. R. Arehart, H.-L. Huang, A. Genc, S. A. Ringel, C. G. Van de Walle, D. A. Muller, and J. Hwang, Phys. Rev. X 9, 041027 (2019).
- <sup>41</sup>A. Portoff, A. Venzie, Y. Qin, M. Stavola, W. B. Fowler, and S. J. Pearton, ECS J. Solid State Sci. Technol. 9, 125006 (2020).

- 46S. A. Kislenko, M. S. Vlaskin, and A. Z. Zhuk, Solid State Ionics 293, 1–6 (2016).
   47T. J. Turner and J. H. Crawford, Jr., Solid State Commun. 17, 167 (1975).
- 48 A. R. Moon and M. R. Phillips, J. Phys. Chem. Solids **52**, 1087 (1991).

- <sup>49</sup>R. Ramírez, R. González, I. Colera, and Y. Chen, Phys. Rev. B 55, 237 (1997).
  <sup>50</sup>G. Zhang, Y. Lu, and X. Wang, Phys. Chem. Chem. Phys. 16, 17523 (2014).
  <sup>51</sup>M. Choi, A. Janotti, and C. G. Van de Walle, ACS Appl. Mater. Interfaces 6, 4149 (2014).

 <sup>&</sup>lt;sup>42</sup>H. J. von Bardeleben, S. Zhou, U. Gerstmann, D. Skachkov, W. R. L. Lambrecht, Q. Ho, and P. Deak, APL Mater. 7, 022521 (2019).
 <sup>43</sup>D. Skachkov, W. R. L. Lambrecht, H. J. von Bardeleben, U. Gerstmann, Q. D.

Ho, and P. Deák, J. Appl. Phys. 125, 185701 (2019).

<sup>44</sup> C. R. A. Catlow, J. Corish, J. Hennessy, and W. C. Mackrodt, J. Am. Ceram. Soc. 71, 42 (1988).

**<sup>45</sup>**Y. Lei and G. Wang, Scr. Mater. **101**, 20 (2015).